Cannabis sativa L. Extract Attenuates UVB-Induced Oxidative Stress and Rescues MITF Transcriptional Suppression in B16-F10 Melanoma Cell Line

Pakawadee Mahaprom
Mahidol University
Kannapat Narasuwan
Mahidol University
Natta Wiriyakun
National Science and Technology Development Agency
Piyanee Ratanachamnong
Mahidol University
Porntipa Korprasertthaworn
Mahidol University
Vasanop Vachiramon
Mahidol University
Pansakorn Tanratana
pansakorn.tan@mahidol.ac.th
Mahidol University

Research Article

Keywords: Hyperpigmentation, Marijuana, Melanin, Melenogenesis, Tetrahydrocannabinol, Tyrosinase

Posted Date: July 1st, 2026

DOI: https://doi.org/10.21203/rs.3.rs-9674603/v1

Additional Declarations: No competing interests reported.

Abstract

Background

Ultraviolet B (UVB) radiation disrupts skin homeostasis through reactive oxygen species (ROS)-mediated oxidative stress and melanogenic imbalance. The search for effective exogenous photoprotectants has highlighted natural products, including *Cannabis sativa* L. phytocannabinoids with reported antioxidant activity. However, their role in UVB-induced cellular responses remains to be clarified.

Methods

Chemical profiling was performed using LC-QTOF-MS and Fourier-transform infrared (FTIR) spectroscopy. Biological activities were assessed in B16-F10 pigmented melanoma cells, including cytotoxicity (MTT assay), intracellular ROS generation (DCFDA assay), transcriptional regulation of melanogenic markers (*MITF*, *TYR*, *TYRP1*, *TYRP2*) by RT-qPCR, and functional melanogenesis outcomes (tyrosinase activity and melanin content).

Results

LC-QTOF-MS revealed that the extract was dominated by neutral cannabinoids, with Δ^9-tetrahydrocannabinol (Δ^9-THC) and cannabinol (CBN) as major constituents. The extract showed moderate free radical scavenging activity in a cell-free DPPH assay. Importantly, pre-treatment with the extract significantly reduced UVB-induced intracellular ROS accumulation. UVB exposure resulted in suppression of *MITF* mRNA expression, which was partially restored at higher extract concentrations, whereas transcript levels of *TYR*, *TYRP1*, and *TYRP2* remained largely unchanged under the experimental conditions. Functionally, the extract attenuated UVB-induced tyrosinase activity at the highest concentration tested, while total melanin content was not significantly altered.

Conclusions

Collectively, these findings suggest that a neutral cannabinoid-rich *C. sativa* extract (CSE) can mitigate UVB-induced oxidative stress and partially restore transcriptional regulation of *MITF* without inducing significant acute depigmentation. The extract may represent a candidate for further investigation as a bioactive component in photoprotective dermatological formulations.

Background

The skin serves as the primary interface between the human body and external environment, continuously exposed to physical and chemical stressors. Among these, UVB radiation (280–320 nm) is a major contributor to acute phototoxic injury and long-term photoaging. UVB exposure induces

excessive generation of ROS, including superoxide anions and hydroxyl radicals, resulting in oxidative damage to lipids, proteins, and nucleic acids (1). These processes contribute to inflammatory signaling, impaired cellular homeostasis, and cumulative tissue dysfunction, collectively referred to as photo-oxidative stress (2).

Melanocytes represent a critical protective cell population in the epidermis primarily through the synthesis and transfer of melanin, which absorbs and scatters UV radiation. However, melanocytes are also highly vulnerable to oxidative stress due to their intrinsic metabolic activity and the pro-oxidant intermediates generated during melanogenesis (3). Acute UVB exposure can disrupt melanocyte regulatory networks, leading to impaired survival signaling and dysregulation of pigmentation pathways (4, 5). Microphthalmia-associated transcription factor (*MITF*) is central to melanocyte biology as it controls melanocyte differentiation, stress adaptation, and melanogenic gene expression. Suppression of *MITF* has been reported as a part of UV-triggered stress responses, and impaired *MITF* signaling, which may compromise melanocyte resilience and pigmentary homeostasis (6, 7). Therefore, strategies capable of mitigating intracellular oxidative stress while preserving *MITF* transcriptional activity may be relevant not only for cosmetic pigmentation outcomes but also for maintaining melanocyte viability under phototoxic conditions.

Natural products have been widely explored as photoprotective candidates due to their diverse antioxidant and anti-inflammatory metabolites (8). *Cannabis sativa L*. has emerged as a particularly rich source of bioactive secondary compounds, including flavonoids, terpenes, and phytocannabinoids such as Δ^9-tetrahydrocannabinol (Δ^9-THC), cannabidiol (CBD), and cannabinol (CBN) (9). Several phytocannabinoids exhibit antioxidant and immunomodulatory properties, and their lipophilic physicochemical characteristics may facilitate membrane interaction and intracellular access to ROS-generating compartments (10, 11). However, current dermatological research has largely focused on isolated cannabinoids (particularly CBD) or acidic cannabinoid-rich extracts, while the biological effects of whole extracts dominated by neutral cannabinoids remain incompletely defined. Importantly, whole plant extracts may exhibit biological activities distinct from single compounds due to combinatorial or synergistic interactions among cannabinoids and minor metabolites (12). In particular, the capacity of neutral cannabinoid-rich extracts to attenuate UVB-induced intracellular oxidative stress and preserve *MITF* transcriptional regulation in pigmented cells remains underexplored. Such mechanisms may be relevant for developing photoprotective strategies that support cellular homeostasis without inducing undesirable depigmentation.

In the present study, we characterized the chemical profile of an ethanolic CSE using LC-QTOF-MS and FTIR spectroscopy and, evaluated its biological effects in a UVB-induced oxidative stress model using B16-F10 pigmented melanoma cells. We assessed cytotoxicity, intracellular ROS generation, transcriptional expression of melanogenic markers, and functional pigmentation outcomes via tyrosinase activity and melanin content assays. Collectively, this work aims to clarify whether a neutral cannabinoid-rich CSE can function as a photochemoprotective modulator of oxidative stress and melanocyte-associated transcriptional regulation under acute UVB exposure.

Materials & Methods

Reagents

Ethanol (Merck, Germany), dimethyl sulfoxide (DMSO) (Panreac, Spain), methanol (Merck, Germany), formic acid (Merck, Germany), acetonitrile (Merck, Germany), sodium hydroxide (NaOH) (Merck, Germany), 2,2-diphenyl-picrylhydrazyl (DPPH) (Sigma-Aldrich, U.S), 3,4-Dihydroxy-L-phenylalanine (L-DOPA) (Sigma-Aldrich, U.S), bovine serum albumin (BSA) (Bio-Rad, U.S.), trypsin-EDTA (Thermo Scientific, U.S.), Dulbecco's modified eagle medium (DMEM, high glucose) (Cytiva, U.S.), fetal bovine serum (FBS) (Cytiva, U.S.), L-glutamine (Cytiva, U.S.), penicillin (Cytiva, U.S.), Reactive Oxygen Species (ROS) Detection Assay Kit (ab287839; Abcam, Cambridge, UK), triton X-100 (Merck, Germany), RIPA buffer (Cell Signaling Technology, U.S.), MTT reagent (Bio Basic, Canada), β-mercaptoethanol (Bio-Rad, U.S.), Bio-Rad protein assay (Bio-Rad, U.S.), Protease inhibitor cocktail (Cell Signaling Technology, U.S.), iScript™ Reverse Transcription Supermix (Bio-Rad, U.S.), Luna® Universal qPCR Master Mix (New England Biolabs, U.S.), β-actin (Gibthai co., Thailand).

Preparation of C. Sativa L. extract

C. sativa L. inflorescence was collected from Phu Seang Thong farm, a private agricultural facility located in Chaiyaphum, Thailand, in August 2023. Explicit permission was obtained from the private landowner to harvest the plant materials for scientific evaluation. The plant material was taxonomically identified by Dr. Sunisa Sangvirotjanapat, Sireeruckhachati Nature Learning Park Project, Mahidol University. A voucher specimen (No. 034/2024) was deposited at Mahidol University (Supplementary Document 1).. Dried inflorescences were ground and extracted with 70% ethanol using ultrasound-assisted extraction (UAE) for 8 h. The supernatant was concentrated using a rotary evaporator (Buchi, German) at 50°C to yield the crude extract. CSE was dissolved in DMSO for biological assays (final DMSO concentration < 0.5%).

Phytochemical Profiling LC-QTOF-MS Analysis

Phytochemicals were analyzed using an ExionLC™ AD system coupled with an X500R QTOF mass spectrometer (Sciex, USA) as previously described (13). Separation was achieved on a Zorbax Eclipse XDB-C18 column (5 µm, 4.6 × 150 mm) at 35°C, using a 0.1% formic acid gradient of water and acetonitrile at 0.5 mL/min. ESI-MS was operated in positive mode (m/z 50–1500) with optimized source parameters: 5500 V spray voltage, 350°C temperature, and 35 ± 15 V collision energy. Data were processed via Sciex OS software and identified using the NIST 2017 library (score ≥ 85%).

Fourier Transform Infrared (FTIR) Spectroscopy Analysis

The functional group profile of CSE was characterized using a Bruker ALPHA FT-IR spectrometer (Bruker, Germany) as previously described (14). The spectra were acquired using the Attenuated Total

Reflectance (ATR) technique. Data were recorded over the wavenumber range of 4,000–400 cm^{-1} with a spectral resolution of 4 cm^{-1} and an accumulation of 32 scans per sample. The resulting spectra were baseline-corrected and analyzed to identify characteristic vibrational bands associated with cannabinoids and phenolic compounds.

DPPH radical scavenging assay

The antioxidant capacity of the extract was evaluated using the 2,2-diphenyl-1-picrylhydrazyl (DPPH) free radical scavenging assay as previously reported with modifications (15). Briefly, 120 µL of CSE at various concentrations was mixed with 1,080 µL of a methanolic DPPH solution. The mixture was incubated in the dark at room temperature for 15 min. The absorbance was subsequently measured at 515 nm using a spectral scanning multimode reader (VarioskanFlash, U.S.). The percentage of radical scavenging activity was calculated using the following equation:

$$\%Inhibition = \frac{Absorbance_{Control} - Absorbance_{Sample}}{Absorbance_{Control}} \times 100$$

Where $Absorbance_{Control}$ is the absorbance of the DPPH solution without CSE, and $Absorbance_{Sample}$ is the absorbance of the reaction mixture containing CSE. The IC_{50} value (concentration required to scavenge 50% of DPPH radicals) was calculated from the non-linear regression analysis of the dose-response curve **(Supplementary Fig. 1).**

Cell Culture and UVB Irradiation

The B16-F10 murine melanoma cell line used in this study was generously provided as a gift by Assoc. Prof. Dr. Prasit Suwannalert from the Department of Pathobiology, Faculty of Science, Mahidol University (Bangkok, Thailand), and was originally sourced from the American Type Culture Collection (ATCC, Manassas, VA, USA) under the repository number CRL-6475. B16-F10 murine melanoma cells were maintained in DMEM high glucose supplemented with 10% FBS, 1% L-glutamine, and 1% penicillin/streptomycin. Cells were cultured at 37°C in a humidified incubator with 5% CO_2 and were routinely sub-cultured using trypsin-EDTA upon reaching approximately 70–80% confluence.

For UVB irradiation experiments, cells were seeded in appropriate culture plates and allowed to adhere overnight. Prior to irradiation, cells were pre-treated with CSE or vehicle control for 30 min. The culture medium was then removed, and cells were gently washed and covered with phosphate-buffered saline (PBS) to avoid UV absorption by phenol red-containing medium. Cells were subsequently exposed to UVB radiation at a dose of 30 mJ/cm² using a UV crosslinker system (CL-508, UVITEC, UK) equipped with 312 nm UVB lamps. Immediately following irradiation, PBS was replaced with fresh complete culture medium, and cells were incubated under standard conditions for 1 h prior to downstream assays.

Cytotoxicity assay

Cytotoxicity of the CSE was evaluated using the MTT assay (16). Briefly, B16-F10 melanoma cells were seeded into 96-well plates at a density of 1×10^4 cells per well and incubated for 24 h at 37°C in a humidified atmosphere containing 5% CO_2 to allow cell attachment. Subsequently, cells were treated with CSE and incubated under the same conditions. Following treatment, MTT solution at final concentration 0.01% was added directly to the medium in each well, and incubated at 37°C for 2 h. Medium was then removed and replaced with DMSO to dissolve the formazan crystals. Absorbance was measured at 570 nm using a spectral scanning multimode reader (VarioskanFlash, U.S.). Cell viability was expressed as a percentage relative to untreated control cells.

Intracellular ROS Quantification

Intracellular ROS levels were measured using the DCFDA assay kit (Abcam, UK) according to the manufacturer's protocol. B16-F10 cells (2.5×10^4 cells/well) were seeded in black 96-well plates and incubated overnight. Cells were stained with DCFDA for 45 min at 37°C in the dark, washed, and pre-treated with CSE for 30 min prior to UVB irradiation (30 mJ/cm²). Fluorescence intensity was measured immediately at Ex/Em = 495/529 nm using a spectral scanning multimode reader (VarioskanFlash, U.S.).

Reverse transcription polymerase chain reaction (RT-qPCR)

Total RNA in B16-F10 cells was extracted with FavorPrep™ Blood/Cultured Cell Total RNA Mini Kit (Favorgen Biotech Corp., Taiwan), and RNA was transcribed reversely into complementary DNA with iScript Reverse Transcription Supermix (Bio-Rad, U.S.) according to the manufacturer's instructions. The RT-qPCR was performed on a CFX Connect detection system (Bio-Rad, U.S.) using Luna® Universal qPCR Master Mix (New England Biolabs, U.S.). All mRNA expression levels were normalized using β-actin (Gibthai co., Thailand). Primer sequences are shown in **Supporting Information Table 1.**

Melanin content and tyrosinase activity

B16-F10 (1.5×10^5 cells) were seeded in 6-well plates. Melanin content was assessed as previously described (17). Briefly, cell pellets were lysed with 1 N NaOH containing 10% DMSO at 80°C for 1 h. The absorbance was measured at 405 nm using a spectral scanning multimode reader (VarioskanFlash, U.S.). The results were normalized to the total protein concentration of the corresponding lysates.

Intracellular tyrosinase activity was determined as previously described (18). Briefly, cell pellets were lysed in Triton X-100 lysis buffer containing 1% protease inhibitor. Lysates containing equal amounts of protein were incubated with 10 mM L-DOPA at 37°C, and dopachrome formation was monitored kinetically by measuring absorbance at 475 nm every 5 min for 1 h.

Statistical analysis

Data are presented as mean ± standard error of the mean (SEM) from three independent experiments. Statistical differences were analyzed using one-way analysis of variance (ANOVA) followed by Dunnett's post-hoc test for multiple comparisons. All analyses were performed using GraphPad Prism 9.5.1 (GraphPad Software, San Diego, CA, USA). A p-value < 0.05 was considered statistically significant.

Results

Phytochemical characterization by LC-QTOF-MS and FTIR spectroscopy of CSE

The reconstructed total ion chromatogram (TIC) from LC-QTOF-MS demonstrated a metabolite profile dominated by late-eluting peaks (retention time at 33–40 min), consistent with enrichment in lipophilic constituents **(**Fig. 1**)**. Compound annotation **(Supporting information Table 2)** revealed that cannabinoids represented the major metabolite class, accounting for 69.44% of the total peak area. The most abundant analytes were identified as Δ⁹-THC (48.23%) and CBN (11.73%), while acidic cannabinoid precursors were detected at substantially lower abundance **(**Fig. 2, **Supporting information Table 2)**.

The functional group profile of the ethanolic CSE was further characterized using ATR-FTIR spectroscopy to provide a structural chemical fingerprint. As shown in Fig. 3, the spectrum displays a broad, intense absorption band at 3,233 cm^{-1}, which is characteristic of O–H stretching vibrations from the phenolic groups inherent in cannabinoids and other polyphenolic constituents. Prominent peaks at 2,924 cm^{-1} correspond to aliphatic C–H stretching, consistent with the long alkyl side chains of neutral cannabinoids like Δ⁹-THC and CBN, which were identified as major components via LC-QTOF-MS. Furthermore, the spectrum exhibits distinct aromatic skeletal vibrations at 1,597 cm^{-1} and 1,515 cm^{-1}, confirming the presence of the phenolic ring structure essential to the cannabinoid framework. The fingerprint region exhibits a significant peak at 1,047 cm^{-1} (C–O stretching), further supporting the presence of a lipophilic terpene-phenolic matrix typical of CSE (19).

Free radical scavenging effect of CSE

The radical scavenging activity of CSE was evaluated using the DPPH assay. The extract demonstrated moderate antioxidant activity, with an IC_{50} value of 133.68 µg/mL.

Cytotoxicity of CSE in B16-F10 melanoma cells

To ensure that the observed photoprotective effects were not confounded by extract-induced cell death, the cytotoxicity of the ethanolic CSE was evaluated using the MTT assay. B16-F10 cells were treated with a broad concentration range (6.25–200 µg/mL) across two exposure windows: a 30-minute pre-treatment and a 1-hour post-irradiation incubation, reflecting the timeline of the UVB challenge experiments. The results demonstrated that CSE treatment did not result in a significant reduction in cell viability compared to untreated controls ($p > 0.05$). Notably, cell viability remained above 80% even at the highest tested concentration of 200 µg/mL **(**Fig. 4**)**. These findings establish that the CSE is well-

tolerated by B16-F10 cells within the experimental dose range. Consequently, subsequent reductions in intracellular ROS and modulation of transcriptional markers can be attributed to biological signaling rather than non-specific cellular toxicity or metabolic collapse.

Effect of CSE on UVB-induced intracellular oxidative stress

To evaluate the photoprotective capacity of the extract, intracellular ROS levels were quantified following acute UVB irradiation (30 mJ/cm²). UVB exposure triggered a robust oxidative response, resulting in a significant surge in ROS accumulation to approximately 200% relative to non-irradiated controls. Pre-treatment with CSE at 25 μg/mL significantly attenuated this UVB-induced ROS generation compared to the irradiated vehicle group (Fig. 5). This marked reduction in fluorescence intensity demonstrates that the neutral cannabinoid-rich extract functions as an effective intracellular antioxidant under phototoxic stress. Given that the extract remained non-cytotoxic at this concentration, these results suggest that CSE actively mitigates the primary driver of UVB-mediated cellular injury rather than simply reflecting a change in cell population density.

Effect of CSE on melanogenic gene expression in UVB-induced B16-F10 cells

To investigate the transcriptional impact of the extract under phototoxic conditions, *MITF* mRNA levels were quantified via RT-qPCR. Acute UVB irradiation (30 mJ/cm²) resulted in a significant suppression of *MITF* expression compared to non-irradiated controls. Pre-treatment with CSE demonstrated a dose-dependent restorative trend. Specifically, a statistically significant rescue of *MITF* transcripts was achieved at the highest concentration of 100 μg/mL ($p < 0.05$), whereas lower concentrations (25 and 50 μg/mL) did not significantly reverse the suppression (Fig. 6A).

To determine if this restoration affected the wider melanogenic pathway, the expression of downstream enzymes was evaluated. Interestingly, transcript levels of *TYR*, *TYRP1*, and *TYRP2* remained stable across all experimental groups, with no statistically significant changes observed following either UVB exposure or CSE treatment under the tested conditions (Figs. 6B–6D).

Effect on tyrosinase activity and melanin synthesis

Functional outcomes of the extract were assessed through enzymatic and pigmentary assays. UVB irradiation significantly elevated intracellular tyrosinase activity. CSE pre-treatment exhibited a dose-dependent inhibitory effect, reaching statistical significance at 100 μg/mL (Fig. 7).

Regarding pigment accumulation, UVB exposure significantly increased total melanin content. However, consistent with the stable mRNA levels of the *TYR* gene family, CSE treatment at concentrations of 25–100 μg/mL did not significantly reduce melanin content compared to the UVB-irradiated vehicle group

(Fig. 8). These results suggest that the extract modulates acute oxidative and enzymatic stress responses without inducing significant acute depigmentation.

Discussion

This study provides a comprehensive characterization of the photochemoprective properties of a neutral cannabinoid-rich CSE against acute UVB-induced stress. Our findings demonstrate that while the extract possesses moderate antioxidant capacity in chemical assays, its biological efficacy in a cellular environment is profound, specifically in the mitigation of ROS and the stabilization of the master melanogenic regulator, *MITF*.

The phytochemical profile established via LC-QTOF-MS and FTIR confirms that the CSE is dominated by neutral phytocannabinoids, specifically Δ^9-THC and CBN. The FTIR spectrum (Fig. 3) serves as a critical structural validator; the intense aliphatic C–H stretching at 2,924 cm^{-1} and the aromatic skeleton vibrations at 1,597 and 1,515 cm^{-1} corroborate the presence of a concentrated terpene-phenolic matrix. Interestingly, the CSE exhibited only moderate radical scavenging activity in the cell-free DPPH assay. This discrepancy between chemical and cellular assays is likely due to the high lipophilicity of neutral cannabinoids (20). In a biological system, this lipophilicity facilitates the partitioning of metabolites into the lipid bilayer of cellular membranes, allowing for localized antioxidant activity that cell-free aqueous assays cannot fully capture (21).

Acute UVB irradiation at 30 mJ/cm^2, equivalent to approximately 15 to 30 min of direct midday sun exposure in the summer, triggered a robust oxidative surge, doubling intracellular ROS levels. This oxidative burst is a primary driver of DNA damage and signal transduction interference (22). The significant reduction of ROS by CSE pre-treatment (Fig. 5) suggests that the extract acts as a primary defense barrier, neutralizing radicals before they can trigger downstream degradative pathways. Notably, the extract was non-cytotoxic throughout the tested concentration range, confirming that ROS reduction was a result of active biological modulation rather than reduced cell viability or cellular metabolic dysfunction. Taken together, these findings support the interpretation that CSE exerts a genuine cytoprotective effect under acute UVB exposure.

A pivotal observation in this study was the dose-dependent restoration of *MITF* transcription following UVB-induced suppression. *MITF* is widely recognized as a master transcription factor governing a melanocyte lineage identity, survival signaling, and melanogenic regulation. UVB-induced suppression of *MITF* has been described as part of an early stress-adaptive program, where melanocytic transcription is temporarily downregulated in response to severe oxidative aggression (6). Interestingly, a dose-dependent hierarchy was observed: while intracellular ROS level was attenuated at lower concentrations, significant *MITF* rescue required 100 µg/mL (Fig. 6A). This suggests that scavenging ROS alone may be insufficient for immediate transcriptional recovery; higher concentrations may be necessary to modulate the upstream stress-kinase signaling pathways that converge on *MITF* regulation. These results indicate that the extract's antioxidant capacity translates into transcriptional resilience. By maintaining *MITF*

levels, CSE likely preserves the melanocyte's long-term survival and structural integrity, even under the duress of UV exposure.

A noteworthy finding was the lack of corresponding changes in the mRNA levels of *TYR*, *TYRP1*, and *TYRP2*, despite the fluctuations in *MITF*. This dissociation can be explained by the distinct temporal kinetics of these markers. In acute stress models, *MITF* functions as a "rapid response" gene, showing immediate transcriptional sensitivity (23). Conversely, the downstream enzymes of the tyrosinase family are characterized by multiple regulatory pathways beyond MITF, including post-transcriptional control and enzyme stability (7, 24). Therefore, the short exposure window used in this study may capture the initial transcriptional rescue of *MITF* without yet reflecting a shift in the steady-state mRNA levels of its downstream targets.

The functional melanogenesis assays further support this interpretation. UVB exposure significantly increased tyrosinase activity, confirming activation of melanogenic enzymatic machinery. Treatment with CSE significantly attenuated UVB-induced tyrosinase activity at the highest concentration tested, indicating that the extract can suppress enzymatic hyperactivation of pre-existing enzymes associated with UV stress. However, total melanin content was not significantly reduced. This divergence likely reflects the kinetic lag between enzymatic modulation and pigment accumulation. Melanin polymerization and intracellular turnover occur over longer timeframes than acute enzymatic changes, and melanin content may remain stable even when tyrosinase activity is partially suppressed in the short term (25). Importantly, preservation of melanin content may be biologically favorable, as melanin provides an essential endogenous photoprotective barrier against UV-induced DNA damage. Thus, the ability of CSE to reduce oxidative stress and dampen enzymatic stress responses without depleting melanin may represent a balanced photoprotective profile.

Collectively, the data supports a conceptual model in which CSE acts primarily as an intracellular oxidative stress modulator that preserves melanocyte-associated transcriptional integrity under UVB exposure **(**Fig. 9.**)**. Rather than functioning as a direct whitening or depigmenting agent, the extract appears to maintain pigmentary stability while reducing oxidative stress burden and supporting transcriptional recovery of *MITF*. This may be particularly relevant for photoprotective or anti-photoaging applications where the goal is to enhance cellular resilience and barrier integrity without compromising physiological pigmentation (26).

While this study provides compelling evidence for the photochemoprotective role of CSE, certain experimental boundaries should be considered when interpreting these findings. First, the use of the B16-F10 melanoma cell line, while a globally recognized and robust model for studying melanogenesis and oxidative stress, represents a transformed cell type with distinct metabolic profiles compared to primary human melanocytes. Future studies utilizing primary cells or 3D reconstructed human skin models would be valuable to further validate the clinical translational potential of these results. Additionally, this research focused on the acute cellular response immediately following UVB exposure. While our data clearly demonstrates that CSE rescues *MITF* transcription and attenuates early enzymatic

hyperactivation, the long-term impact on genomic stability and chronic photoaging remains to be explored. Finally, while we identified neutral cannabinoids as the primary bioactive constituents through LC-QTOF-MS and FTIR, the potential synergistic "entourage effect" between these cannabinoids and minor terpenes or flavonoids in the extract warrants further investigation via bioassay-guided fractionation.

Despite these limitations, the consistency across our chemical, transcriptional, and functional assays provides a strong foundational proof-of-concept for the use of *Cannabis sativa* L. extracts as active agents in dermatological photoprotection.

Conclusion and Future Direction

In conclusion, this study establishes that an ethanolic CSE, characterized by a lipophilic terpene-phenolic matrix of neutral cannabinoids, serves as a potential cytoprotective modulator against UVB-induced oxidative injury. Our data demonstrates that CSE effectively neutralizes intracellular ROS accumulation and rescues the transcriptional suppression of *MITF*, acting as a biological shield that prevents enzymatic hyperactivation without inducing acute depigmentation or disrupting the skin's natural melanin barrier. Moving forward, transitioning from 2D monolayers to 3D reconstructed human skin models and elucidating the specific upstream signaling kinases (e.g., MAPK pathways) involved in *MITF* resilience will be critical to translating these foundational findings into advanced dermaceutical formulations. By bridging chemical profiling with molecular resilience, these results provide a strong mechanistic roadmap for utilizing cannabis-derived extracts to enhance skin homeostasis against solar radiation.

Abbreviations

UVB
ultraviolet B
ROS
reactive oxygen species
LC-QTOF-MS
liquid chromatography–quadrupole time-of-flight mass spectrometry
FTIR
Fourier-transform infrared spectroscopy
MTT
(3-(4,5-dimethylthiazol-2-yl)-2,5-diphenyltetrazolium bromide) assay
DCFDA
2',7'-dichlorofluorescein diacetate
RT-qPCR
reverse transcription quantitative polymerase chain reaction
MITF

microphthalmia-associated transcription factor
TYR
tyrosinase
TYRP1
tyrosinase-related protein 1
TYRP2
tyrosinase-related protein 2
Δ^9-THC
delta-9-tetrahydrocannabinol
CBN
cannabinol
CBD
cannabidiol
DPPH
2,2-diphenyl-1-picrylhydrazyl
DMSO
dimethyl sulfoxide
NaOH
sodium hydroxide
BSA
bovine serum albumin
DMEM
Dulbecco's Modified Eagle Medium
FBS
fetal bovine serum
PBS
phosphate-buffered saline
UAE
ultrasound-assisted extraction
ESI-MS
electrospray ionization mass spectrometry
m/z
mass-to-charge ratio
NIST
National Institute of Standards and Technology
ATR
attenuated total reflectance
IC_{50} (IC50)
half maximal inhibitory concentration
SEM

standard error of the mean
ANOVA
analysis of variance
CO_2
carbon dioxide
TIC
total ion chromatogram
CSE
Cannabis sativa extract
RIPA
radioimmunoprecipitation assay (buffer).

Declarations

Ethical approval and consent to participate

- Not applicable

Consent for publication

- Not applicable

Competing interests

The authors declare that they have no competing interests.

Funding

Scholarship for postgraduate Study for Graduates of Bachelor of Science Program in Biomedical Sciences (International Program), Faculty of Science, Mahidol University, Bangkok, Thailand.

Author Contribution

PM performed the majority of the experimental work, including preparation of CSE, cell culture, ROS assays, RT-qPCR, and enzymatic assays, and drafted the initial manuscript. KN contributed to the experimental design and assisted in data collection and technical support. NW performed the LC-QTOF-MS analysis and interpreted the phytochemical data. PR assisted in the plant extraction and optimized the sample preparation process. PK and VV critically reviewed the manuscript and provided essential clinical and pharmacological insights. PT conceptualized the study, secured funding, supervised the

research, and performed the final drafting and revision of the manuscript. All authors have read and approved the final version of the manuscript.

Acknowledgement

The authors would like to express their sincere gratitude to Dr. Yamaratee Jaisin (Department of Pharmacology, Faculty of Medicine, Srinakharinwirot University) for her generous support in providing access to the spectrophotometer used in this study.

Data Availability

All data generated or analyzed during this study are included in this published article and its supplementary information files.

References

1. Gupta A, Avci P, Dai T, Huang Y-Y, Hamblin M. Ultraviolet Radiation in Wound Care: Sterilization and Stimulation. Adv Wound Care. 2013;2:422–37.
2. Amaro-Ortiz A, Yan B, D'Orazio JA. Ultraviolet radiation, aging and the skin: prevention of damage by topical cAMP manipulation. Molecules. 2014;19(5):6202–19.
3. Denat L, Kadekaro AL, Marrot L, Leachman SA, Abdel-Malek ZA. Melanocytes as instigators and victims of oxidative stress. J Invest Dermatol. 2014;134(6):1512–8.
4. Chen H, Weng QY, Fisher DE. UV Signaling Pathways within the Skin. J Invest Dermatol. 2014;134(8):2080–5.
5. Costin GE, Hearing VJ. Human skin pigmentation: melanocytes modulate skin color in response to stress. FASEB J. 2007;21(4):976–94.
6. Malcov-Brog H, Alpert A, Golan T, Parikh S, Nordlinger A, Netti F, et al. UV-Protection Timer Controls Linkage between Stress and Pigmentation Skin Protection Systems. Mol Cell. 2018;72(3):444–e567.
7. D'Mello SA, Finlay GJ, Baguley BC, Askarian-Amiri ME. Signaling Pathways in Melanogenesis. Int J Mol Sci. 2016;17(7).
8. Li L, Chong L, Huang T, Ma Y, Li Y, Ding H. Natural products and extracts from plants as natural UV filters for sunscreens: A review. Anim Model Exp Med. 2023;6(3):183–95.
9. Flores-Sanchez IJ, Verpoorte R. Secondary metabolism in cannabis. Phytochem Rev. 2008;7(3):615–39.
10. Gagné V, Boucher N, Desgagné-Penix I. Cannabis Roots: Therapeutic, Biotechnological and Environmental Aspects. Cannabis Cannabinoid Res. 2024;9(1):35–48.
11. Kopustinskiene DM, Masteikova R, Lazauskas R, Bernatoniene J. Cannabis sativa L. Bioactive Compounds and Their Protective Role in Oxidative Stress and Inflammation. Antioxid [Internet].

2022; 11(4).

12. André R, Gomes AP, Pereira-Leite C, Marques-da-Costa A, Monteiro Rodrigues L, Sassano M et al. The Entourage Effect in Cannabis Medicinal Products: A Comprehensive Review. Pharmaceuticals (Basel). 2024;17(11).
13. Tangpudtasiri P, Wiriyakun N, Niwaspragrit C, Amornlerdpison D, Namchaiw P, Ratanachamnong P, et al. The Effect of Uvaria rufa Fruit Extract for Antioxidant and Anti-Melanogenic Activities and Phytochemical Profiling Using LC–MS Analysis. J Med Food. 2025;29(1):22–32.
14. Al-Amin K, Kawsar M, Mamun M, Sahadat Hossain M. Fourier transform infrared spectroscopic technique for analysis of inorganic materials: a review. Nanoscale Adv. 2025;7(21):6677–702.
15. Kedare SB, Singh RP. Genesis and development of DPPH method of antioxidant assay. J Food Sci Technol. 2011;48(4):412–22.
16. van Meerloo J, Kaspers GJ, Cloos J. Cell sensitivity assays: the MTT assay. Methods Mol Biol. 2011;731:237–45.
17. Hu D-N. Methodology for Evaluation of Melanin Content and Production of Pigment Cells in Vitro. Photochem Photobiol. 2008;84(3):645–9.
18. Panich U, Kongtaphan K, Onkoksoong T, Jaemsak K, Phadungrakwittaya R, Thaworn A, et al. Modulation of antioxidant defense by Alpinia galanga and Curcuma aromatica extracts correlates with their inhibition of UVA-induced melanogenesis. Cell Biol Toxicol. 2010;26(2):103–16.
19. Jin D, Henry P, Shan J, Chen J. Identification of Chemotypic Markers in Three Chemotype Categories of Cannabis Using Secondary Metabolites Profiled in Inflorescences, Leaves, Stem Bark, and Roots. Front Plant Sci. 2021;12:699530.
20. Maccarrone M, Bab I, Bíró T, Cabral GA, Dey SK, Di Marzo V, et al. Endocannabinoid signaling at the periphery: 50 years after THC. Trends Pharmacol Sci. 2015;36(5):277–96.
21. Pereira Sónia R, Hackett B, O'Driscoll David N, Sun Melody C, Downer Eric J. Cannabidiol modulation of oxidative stress and signalling. Neuronal Signal. 2021;5(3):NS20200080.
22. Gocek-Szczurtek N, Żabka A, Wróblewski M, Polit JT. Stabilization of the MAPK-Epigenetic Signaling Axis Underlies the Protective Effect of Thyme Oil Against Cadmium Stress in Root Meristem Cells of Vicia faba. Int J Mol Sci. 2025;27(1).
23. Mizutani Y, Hayashi N, Kawashima M, Imokawa G. A single UVB exposure increases the expression of functional KIT in human melanocytes by up-regulating MITF expression through the phosphorylation of p38/CREB. Arch Dermatol Res. 2010;302(4):283–94.
24. Hida T, Kamiya T, Kawakami A, Ogino J, Sohma H, Uhara H et al. Elucidation of Melanogenesis Cascade for Identifying Pathophysiology and Therapeutic Approach of Pigmentary Disorders and Melanoma. Int J Mol Sci. 2020;21(17).
25. Cichorek M, Wachulska M, Stasiewicz A, Tymińska A. Review paperSkin melanocytes: biology and development. Adv Dermatology Allergology/Postępy Dermatologii i Alergologii. 2013;30(1):30–41.

26. Rinnerthaler M, Bischof J, Streubel MK, Trost A, Richter K. Oxidative stress in aging human skin. Biomolecules. 2015;5(2):545–89.

Figures

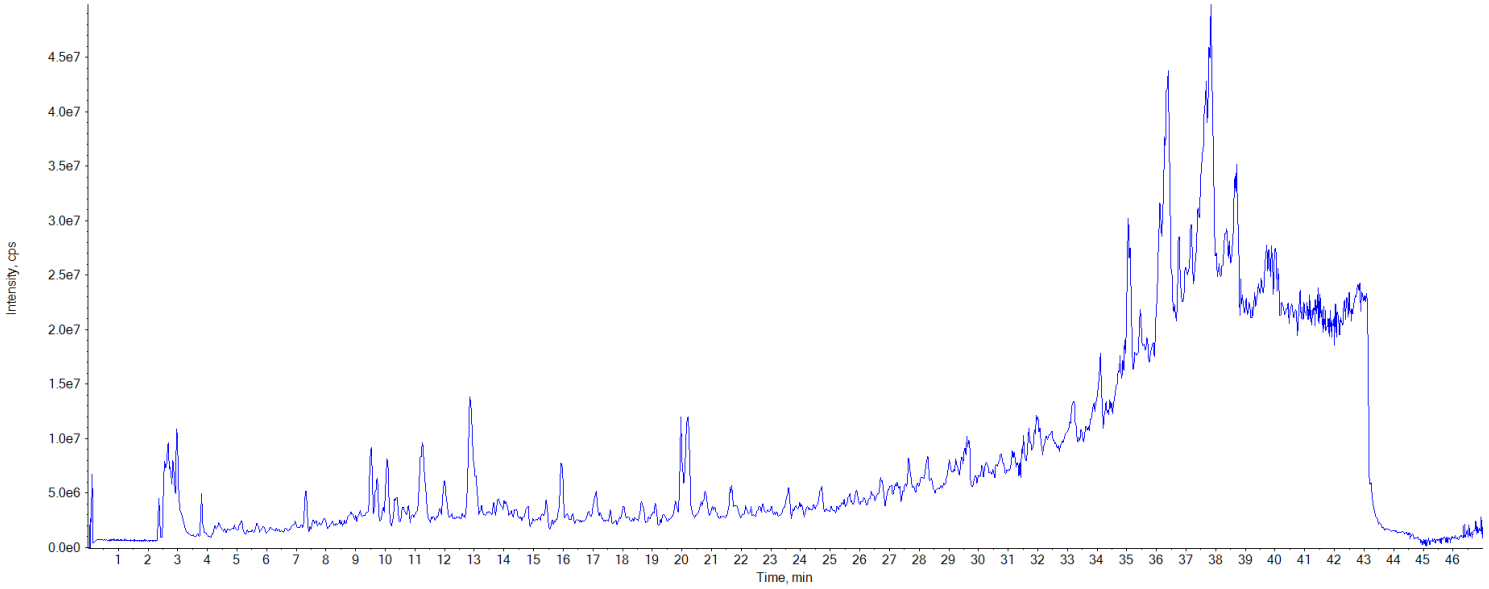

Figure 1

LC-QTOF-MS total ion chromatogram of the ethanolic CSE. Representative TIC acquired in positive electrospray ionization (ESI+) mode. The prominent cluster of metabolites eluting between 33 and 40 minutes indicates a high concentration of non-polar constituents, providing a comprehensive overview of the extract's complex phytochemical matrix.

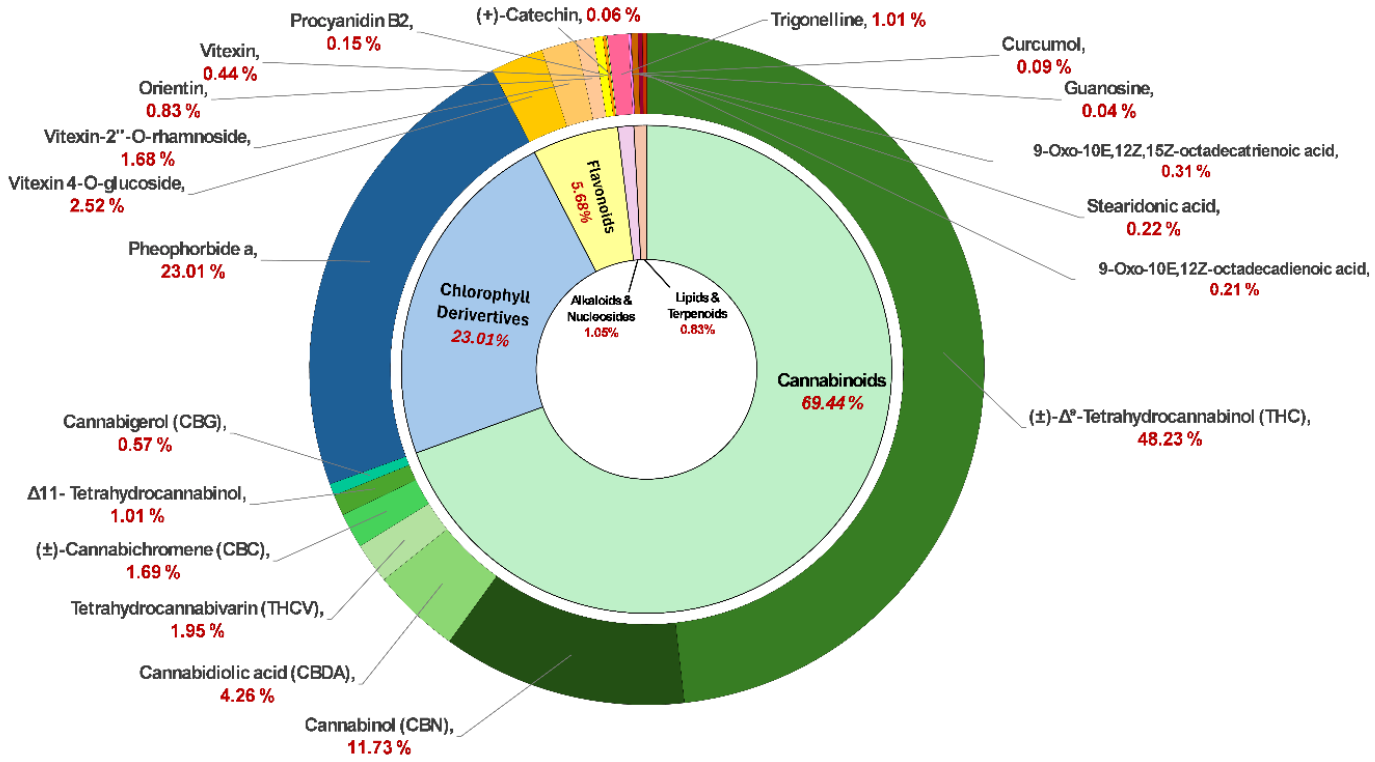

Figure 2

Quantitative distribution of phytochemical classes and major metabolites in CSE. A sunburst hierarchy illustrating relative metabolite abundance based on LC-QTOF-MS peak area integration. The inner ring identifies chemical classes, while the outer ring specifies individual compounds. Cannabinoids represent the dominant fraction, with Δ⁹-THC) and CBN identified as the primary constituents.

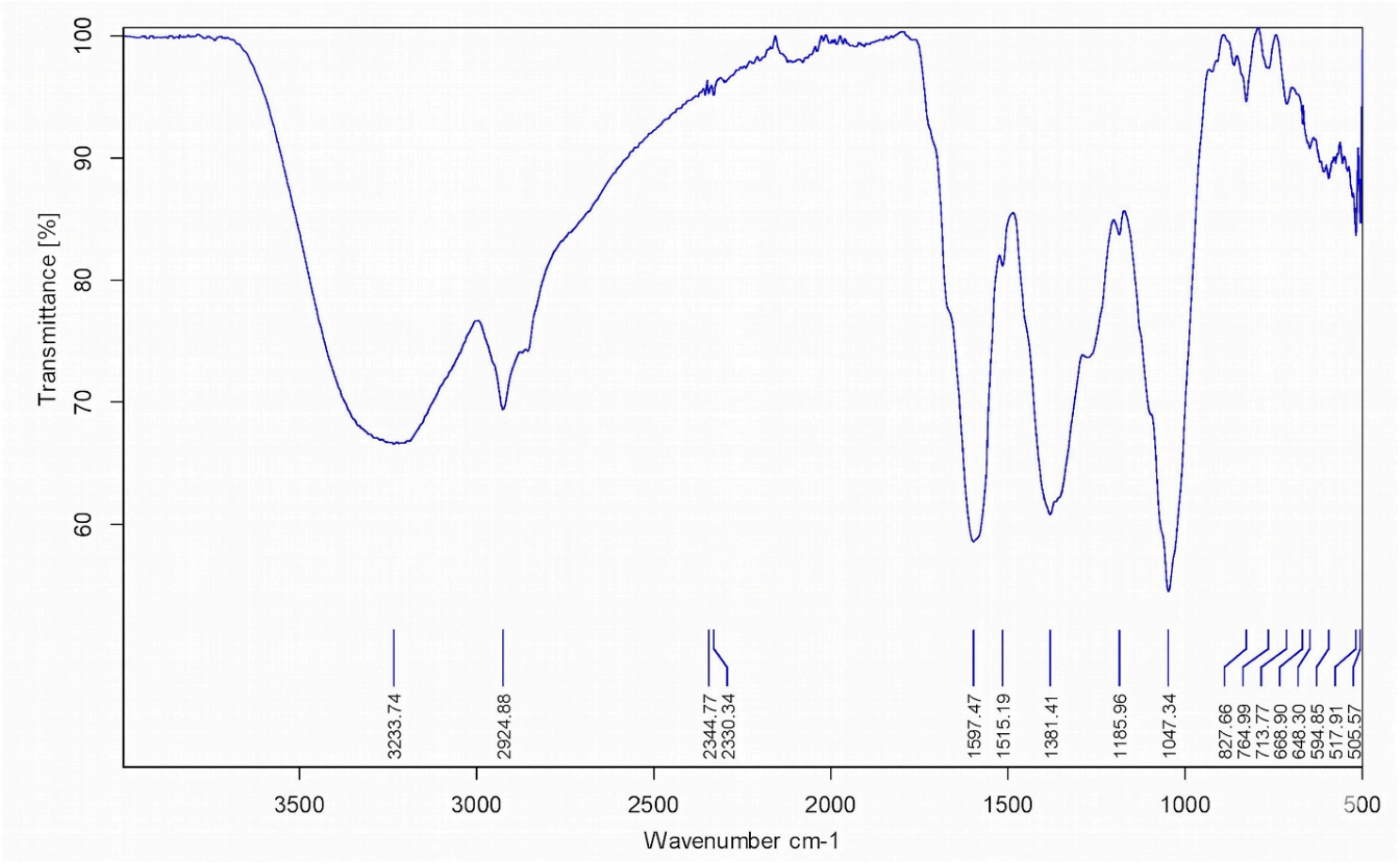

Figure 3

ATR-FTIR spectroscopic profile of the ethanolic CSE. Structural fingerprinting obtained via ATR-FTIR (4,000–400 cm^{-1}). Key vibrational bands include phenolic/hydroxyl (O–H) stretching at 3,233 cm^{-1}, aliphatic C–H stretching at 2,924 cm^{-1}, and aromatic C=C skeletal vibrations at 1,597 and 1,515 cm^{-1}. The prominence of these aliphatic and aromatic signals confirms a highly lipophilic terpene-phenolic matrix, supporting the extract's capacity for intracellular partitioning and localized antioxidant activity.

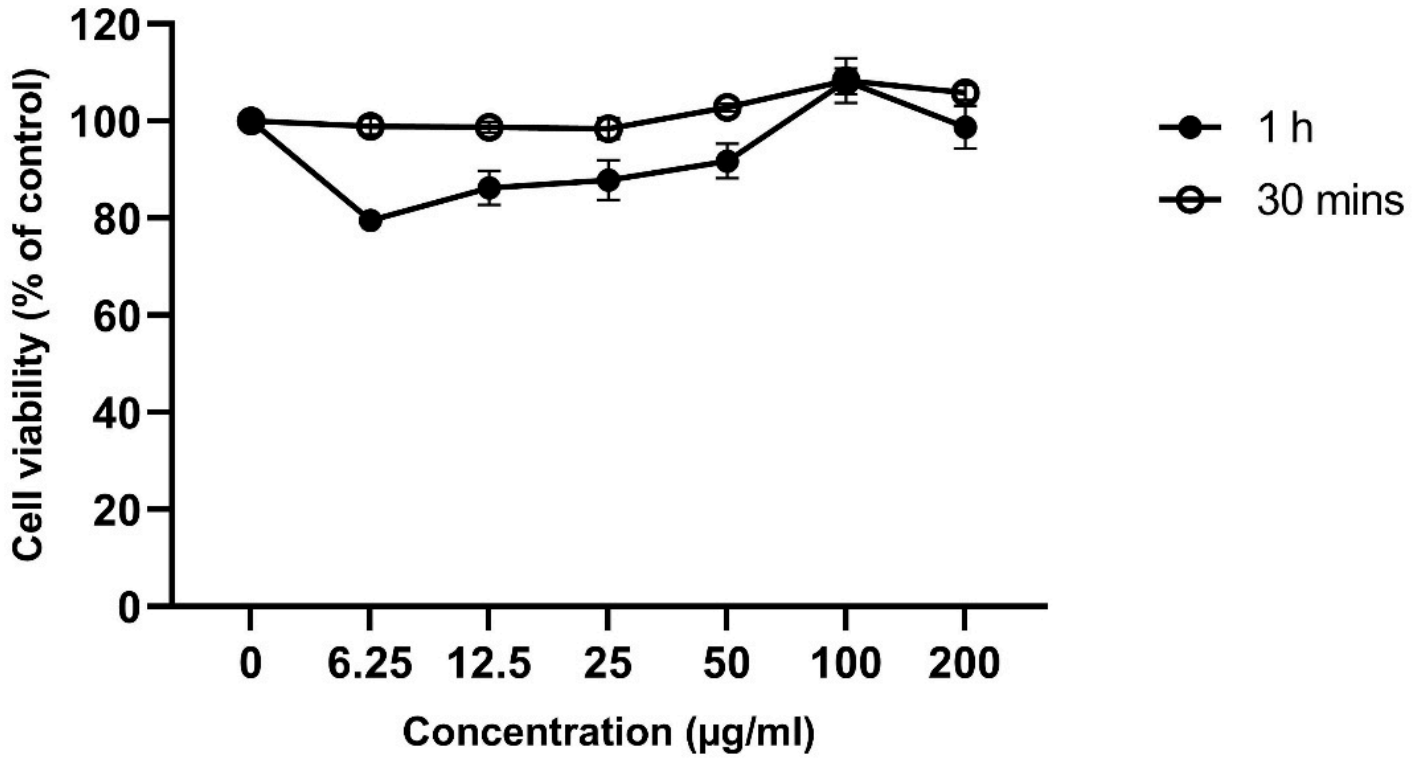

Figure 4

Cytotoxicity profile of the ethanolic CSE on B16-F10 melanoma cells. Cell viability was assessed by MTT assay following exposure to CSE (6.25–200 µg/mL) for 30 min and 1 h to mirror experimental UVB challenge conditions. Data are presented as mean ± SEM (n=3). No significant reduction in viability was observed ($p > 0.05$), establishing the non-cytotoxic range for subsequent assays.

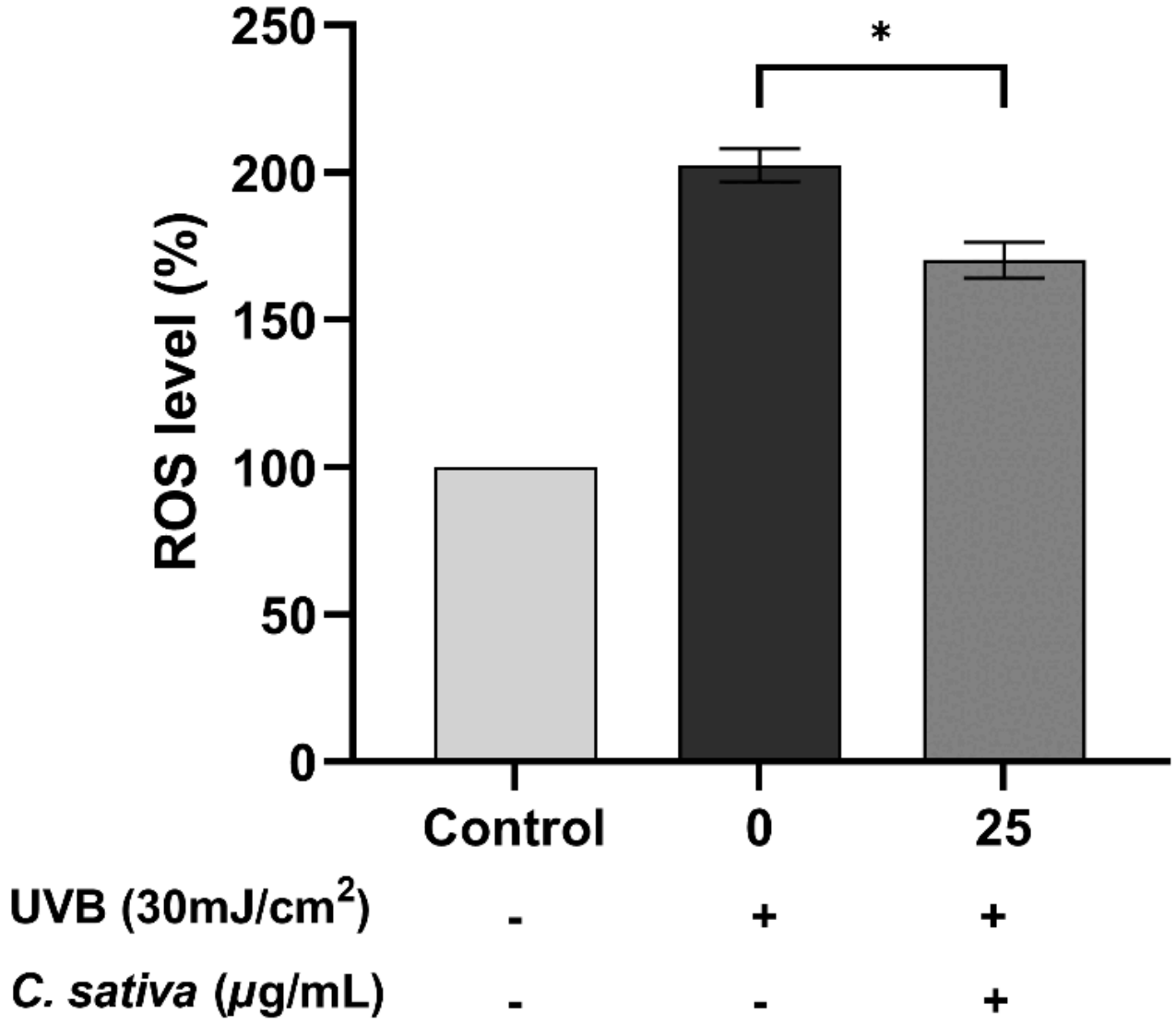

Figure 5

Attenuation of UVB-induced intracellular ROS accumulation by CSE. Intracellular ROS levels were quantified using the DCFH-DA fluorometric probe 1 h post-UVB irradiation (30 mJ/cm²). CSE pre-treatment (25 µg/mL) significantly suppressed the oxidative burst compared to the irradiated vehicle group. Data are normalized to non-irradiated controls (mean ± SEM, $n=3$). * indicates $p < 0.05$.

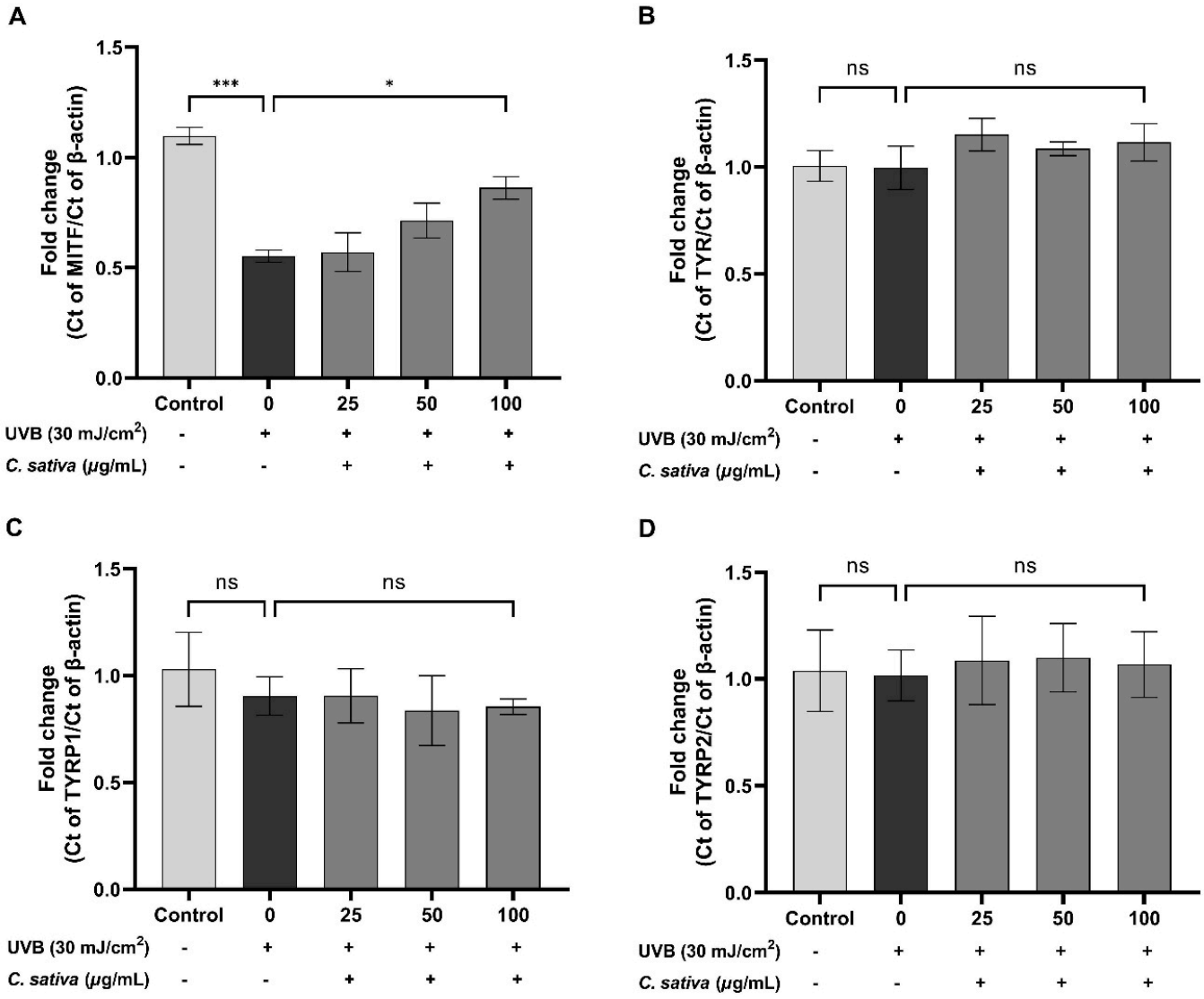

Figure 6

Impact of CSE on the transcriptional regulation of melanogenic markers. Relative mRNA expression of (A) *MITF*, (B) *TYR*, (C) *TYRP1*, and (D) *TYRP2* was determined via RT-qPCR 24 h post-UVB irradiation (30 mJ/cm²). Data were normalized to the housekeeping gene β-actin and are presented as fold change relative to the control (mean ± SEM, n = 3). * indicates $p < 0.05$, *** indicates $p < 0.001$; ns = not significant.

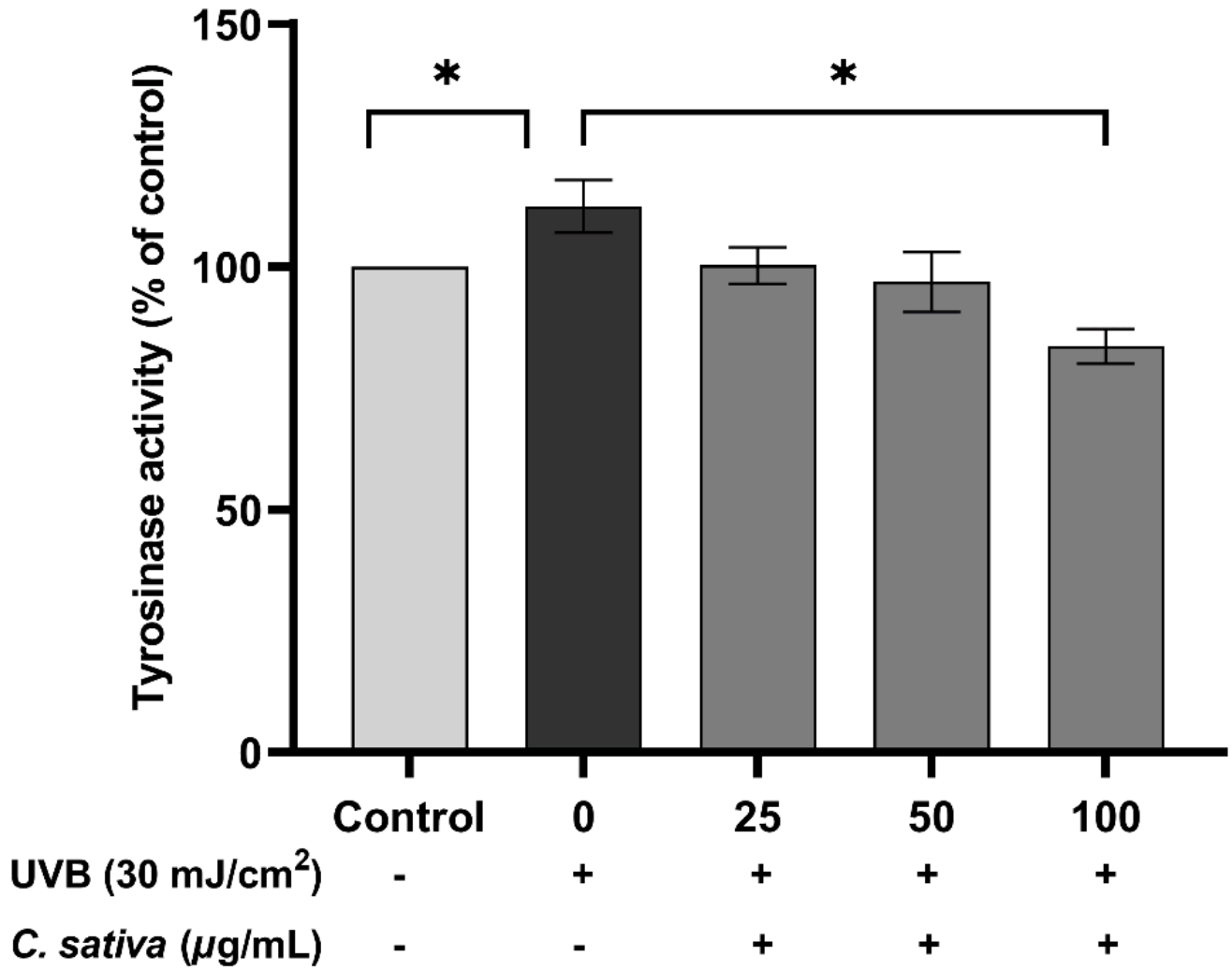

Figure 7

Inhibition of UVB-induced cellular tyrosinase activity by CSE. Functional enzymatic activity was determined by the rate of L-DOPA oxidation in cell lysates. CSE pre-treatment dose-dependently attenuated the enzymatic hyperactivation triggered by acute UVB exposure. Results are normalized to total protein content (mean ± SEM, $n = 3$). * indicates $p < 0.05$.

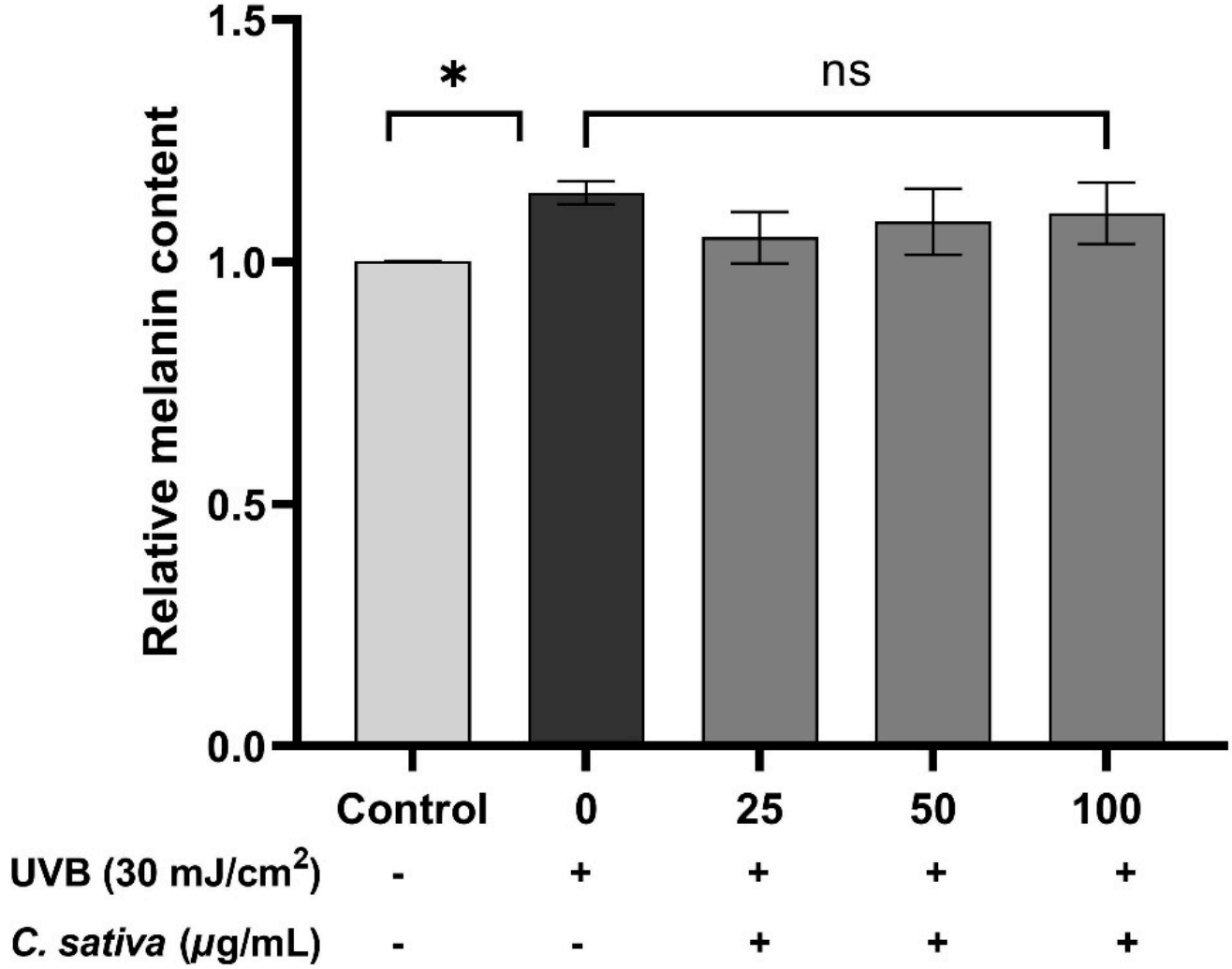

Figure 8

Effect of CSE on melanin content following UVB challenge. Total melanin was quantified spectrophotometrically at 405 nm and normalized to total protein. Despite modulation of upstream markers, CSE treatment did not significantly alter absolute pigment levels compared to the irradiated vehicle. Data are presented as relative fold change (mean ± SEM, $n = 3$). * indicates $p < 0.05$; ns = not significant

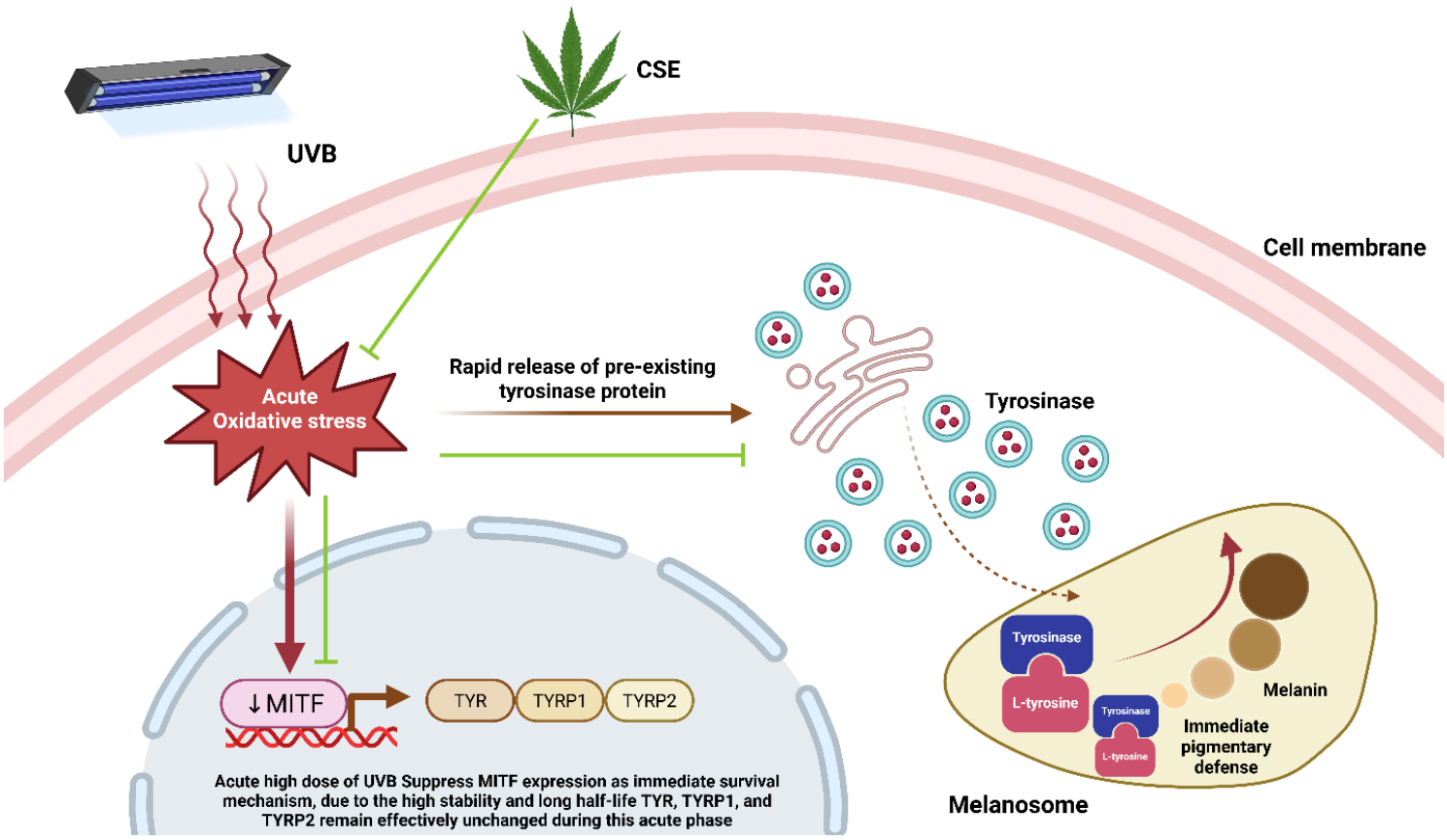

Figure 9

Proposed mechanism of CSE-mediated photochemoprotection. Schematic model illustrating the cytoprotective role of CSE. Acute UVB induces an oxidative burst that suppresses *MITF* transcription and mobilizes tyrosinase. Lipophilic CSE scavenges these initial ROS (green inhibitory lines), thereby preventing enzymatic hyperactivation and mitigating *MITF* downregulation to maintain cellular homeostasis and pigmentary stability under UV stress.

Supplementary Files

This is a list of supplementary files associated with this preprint. Click to download.

- Supplementaryfile.docx